

Supporting Information

Ammonia decomposition for H₂ production over an iron catalyst in a molten barium amide

Haojun Li, Li Rao*, Sheng Feng, Wenbo Gao, Jiemin Wang, Yanbo Deng, Xuanwei Chang, Lin Liu, Teng He, Jianping Guo*, and Ping Chen

H. Li, S. Feng, W. Gao, J. Wang, Y. Deng, X. Chang, L. Liu, T. He, J. Guo, P. Chen
Dalian Institute of Chemical Physics, Chinese Academy of Sciences, Dalian 116023,
China

E-mail: guojianping@dicp.ac.cn

H. Li, W. Gao, X. Chang, L. Liu, T. He, J. Guo, P. Chen
Center of Materials and Optoelectronics Engineering, University of Chinese Academy
of Sciences, Beijing 100049, China

L. Rao

State Key Laboratory of Green Pesticide, College of Chemistry, Central China
Normal University, Wuhan 430079, China.

E-mail: raoli@mail.ccnu.edu.cn

This PDF file includes:

Materials and Methods

Figures S1 to S9

Tables S1 to S3

References

Materials and Methods

1. Preparation of alkaline earth metal amides

$\text{Mg}(\text{NH}_2)_2$ was synthesized by reacting metallic Mg powder (Sigma-Aldrich, 99%) with pure NH_3 (Dalian CREDIT, 99.999%) at 300 °C for ca. 200 h^[1]. $\text{Ca}(\text{NH}_2)_2$, $\text{Ba}(\text{NH}_2)_2$, and $\text{Sr}(\text{NH}_2)_2$ were prepared by reacting Ca (Alfa-Aesar, 99%), Ba (Macklin, 99%) and Sr (ZhongNuo Advanced Materials, 99.8%) metals with liquid NH_3 in closed systems at room temperature for ca. 4 days^[2-3]. LiNH_2 was purchased from Alfa-Aesar (95%). All the sample handlings were conducted in a glove box filled with purified argon to keep a low moisture concentration (< 1 ppm) and a low oxygen concentration (< 1 ppm).

2. Catalyst synthesis

The Fe- $\text{Ba}(\text{NH}_2)_2$, Fe- $\text{Ca}(\text{NH}_2)_2$, Fe- $\text{Mg}(\text{NH}_2)_2$, Fe- $\text{Sr}(\text{NH}_2)_2$ and Fe- LiNH_2 composite catalysts were prepared by grinding $\text{Fe}_2(\text{CO})_9$ (Macklin, 97%) and self-made alkaline earth metal amides or commercial lithium amide, i.e., $\text{Ba}(\text{NH}_2)_2$, $\text{Ca}(\text{NH}_2)_2$, $\text{Mg}(\text{NH}_2)_2$, $\text{Sr}(\text{NH}_2)_2$ and LiNH_2 in an agate mortar and pestling for ca. 20 min. The Co- $\text{Ba}(\text{NH}_2)_2$ and Ni- $\text{Ba}(\text{NH}_2)_2$ were synthesized by grinding $\text{Co}_2(\text{CO})_8$ (J&K, 95%) or Ni(Cp)₂ (Aladdin, 98%) and $\text{Ba}(\text{NH}_2)_2$ in an agate mortar and pestling for ca. 20 min. These samples were annealed under ammonia gas at 250 °C for 1 hour to remove carbonyl groups.

The 6wt% Fe/MgO reference catalyst was prepared via two different methods, i.e., co-precipitation and grinding methods. For the coprecipitation method, $\text{Fe}(\text{NO}_3)_3 \cdot 9\text{H}_2\text{O}$ (Kermel, 98.5%), $\text{K}_2\text{C}_2\text{O}_4 \cdot \text{H}_2\text{O}$ (Kermel, 99%), and MgO (Sinopharm China, 99.9%) were mixed in an aqueous solution and stirred for 12 hours. The obtained solid sample was then dried at 80 °C for 2h. Finally, the sample was then calcined in pure NH_3 at 600 °C for 2 h and was denoted as Fe/MgO. For the grinding method, a procedure similar to that used for the Fe- $\text{Ba}(\text{NH}_2)_2$ sample was employed. In this case, $\text{Fe}_2(\text{CO})_9$ was used as the iron precursor.

3. Activity test

NH_3 decomposition reaction was performed on a continuous-flow fixed-bed U-tube quartz reactor (I.D.: 0.6 cm; length: 25 cm) at atmospheric pressure. Typically, 100 mg of catalyst powder was loaded into the quartz reactor, and then heated from room temperature to 250 °C at 5 °C min⁻¹ under a flow of pure NH_3 . The activity was evaluated in the temperature range of 250 to 450 °C and measured with an interval of 50

°C. NH₃ conversion data reported here were collected after ca. 30 min time-on-stream at the corresponding temperatures. The flow rates of pure NH₃ were 10 mL min⁻¹ regulated by a mass flow controller (Sevenstar, model 5850E). NH₃ and N₂ were analyzed by an on-line gas chromatograph (GC-2014C, Shimadzu) equipped with a Porapak N column and a thermal conductivity detector, using H₂ as the carrier gas. During the catalytic testing, the exhaust gas composition including the unconverted NH₃ and produced H₂, N₂, were examined. According to the standard curve of GC peak area as a function of NH₃ concentration, the NH₃ conversion can be determined.

4. Characterization

X-ray Diffraction (XRD) measurements:

Phase identification of samples was performed by a PANalytical X'pert diffractometer with Cu K_α radiation at 40 kV and 40 mA. A self-made sample cell covered with KAPTON film was used to protect sample from air or moisture contamination.

Ar-Temperature-Programmed-Decomposition (Ar-TPD):

The gaseous products from samples during the heating process were measured by using a homemade Ar-TPD system equipped with an online mass spectrometer (Hiden HPR-20), which recorded the signals of H₂ ($m/z = 2$), N₂ ($m/z = 28$), and NH₃ ($m/z = 17$) simultaneously. Pure Ar was used as the carrier gas (30 mL min⁻¹). In each test, 30 mg of sample was loaded into the U-tube quartz reactor and heated from room temperature to 500 °C at 2 °C min⁻¹.

FTIR measurements were conducted on a Tensor II FTIR spectrometer in the diffuse reflection mode. The sample was loaded into a ceramic crucible and enclosed in an in situ heat chamber for DiffusIRTM accessory with KBr window slice (purchased from PIKE Technologies).

Scanning electron microscopy (SEM) and energy-dispersive X-ray spectrometry (EDX):

The compositions of the catalyst, including spectral imaging to produce elemental maps, were captured using a SEM microscope equipped with an EDX detector.

The XPS measurements were performed using an Escalab 250 Xi X-ray photoelectron spectrometer (Thermo Scientific) with nonmonochromatic Al K_α radiation (photon energy, 1486.6 eV). In order to remove the oxidation layers, the Ar sputtering experiments were performed at a background vacuum of 1×10^{-7} Pa, a sputtering acceleration voltage of 14.2 kV, and a sputtering current of 10.11 mA. Adventitious carbon was used to calibrate the binding energy shifts of the samples (C1s = 284.8 eV).

The depth profile and chemical evolution of Fe-Ba(NH₂)₂ were further analyzed by Time-of-Flight secondary ion mass spectrometry (ToF-SIMS, ToF-SIMS M6 ION-ToF GmbH, Münster, Germany), equipped with a 30 keV Bi⁺ gun (scanning area of 100×100 μm²) for analysis beam, 500 eV Ar⁺ gun (sputtering area of 300×300 μm²) for sputtering beam.

5. The calculation of TOF_{H₂} value

TOF value can be calculated according to Fe loading content and H₂ formation rate of Fe-based sample.

The TOF calculation process is detailed as follows:

For example, Fe loading content is 1 wt%, and H₂ formation rate of Fe-Ba(NH₂)₂ sample is 2.72 mmol_{H₂} g_{cat}⁻¹ min⁻¹ at 400 °C. 1 g catalyst contains the number of Fe atom to be $1.791 \times 10^{-4} N_A$ ($N_A = 6.02 \times 10^{23}$), TOF_{H₂} value (the H₂ formation amount per Fe atom per second) is calculated to be $2.72 \times 10^{-3} N_A / 60 / 1.791 \times 10^{-4} N_A = 0.253 \text{ s}^{-1}$.

6. Computational details

All reactants, intermediates, and transition states were obtained by geometry optimization employing ωB97xD^[4]/6-31G*(lanl2dz for Fe, Co and Ba) level of theory. The nature of stationary points was verified by frequency analysis. Energy correction was performed employing ωB97xD/6-311+G**(SDD for Fe, Co and Ba) level of theory. The temperature for Gibbs free energy calculation was set to be 723 K (450 °C). All calculations were performed using Gaussian09^[5]. We would like to emphasize that barium amide is in a molten state under the temperature of ammonia decomposition experiments (350-450 °C), which is a significant challenge to the identification of the catalytic [Ba-NH_x-Fe] species. Therefore, we theoretically optimized the structures of different Ba_xFe_y(NH₂)_z species as a screening of possible ammonia decomposition catalyst. Energy barriers of two major steps in ammonia decomposition were considered in this screening, the first hydrogen abstraction (HAT) step from (NH₃)₂ to the release of the first H₂ molecule, and the N-N coupling step from (NH₂)₂ to NH₂-NH₂. It should be noticed that since ammonia decomposition is an endothermic reaction, the subsequent HAT steps would be more difficult than the first HAT step. As shown in Table S3, the Ba₂Fe₂(NH₂)₇ species exhibited the best HAT activity with a barrier height of merely 17.4 kcal/mol. Without iron atom, the first HAT barrier height of Ba₄(NH₂)₇ species dramatically increased to 43.3 kcal/mol and likely to be higher in the subsequent HAT steps. However, the N-N coupling barrier height of the Ba₄(NH₂)₇ decreased to 35.2 kcal/mol. Therefore, we conclude that

HAT steps happen on Fe atoms while N-N coupling happen on Ba atoms. Both steps' barrier heights were too high on the $\text{BaFe}(\text{NH}_2)_7$. $\text{Ba}_2\text{Co}_2(\text{NH}_2)_7$ showed not so high HAT and N-N coupling barrier heights, explaining why ternary barium cobalt amide also exhibited some ammonia decomposition activity.

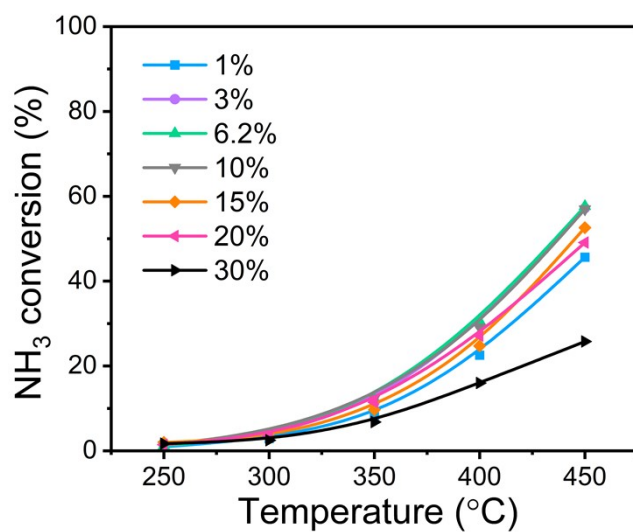


Figure S1. The catalytic performance of $\text{Fe-Ba}(\text{NH}_2)_2$ with different Fe loadings as a function of temperature. Reaction condition: $\text{WHSV} = 6000 \text{ mL}_{\text{NH}_3} \text{ g}_{\text{cat}}^{-1} \text{ h}^{-1}$.

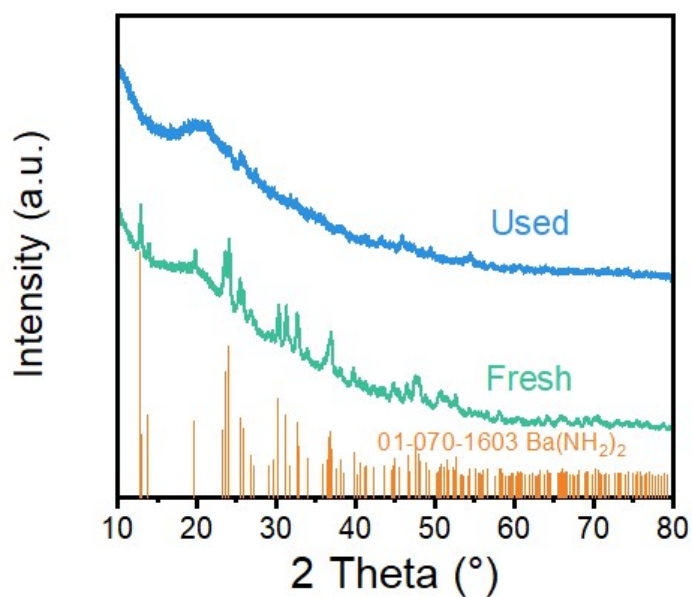


Figure S2. XRD patterns for the fresh and used Fe-Ba(NH₂)₂ catalysts collected after catalytic testing at 400 °C.

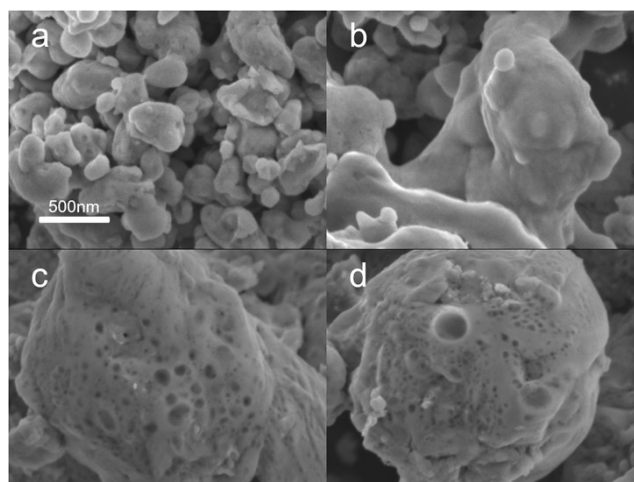


Figure S3. a, b) SEM images of the Fe-Ba(NH₂)₂ catalyst before ammonia decomposition test; c, d) SEM images of the Fe-Ba(NH₂)₂ catalyst collected after ammonia decomposition test.

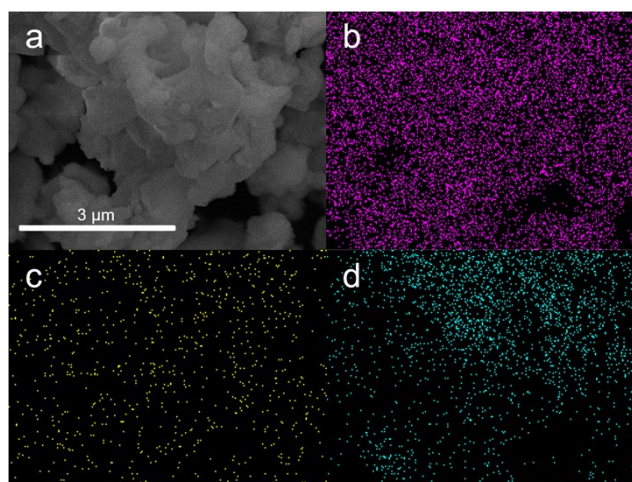


Figure S4. a) SEM image of Fe-Ba(NH₂)₂ catalyst after ammonia decomposition test and EDX elemental mapping of b) Ba, c) Fe, d) N.

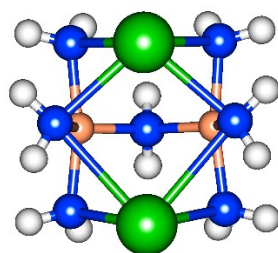
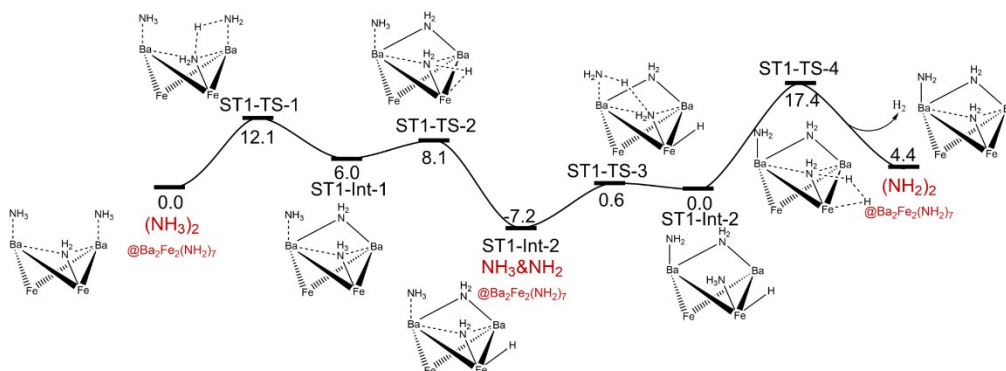
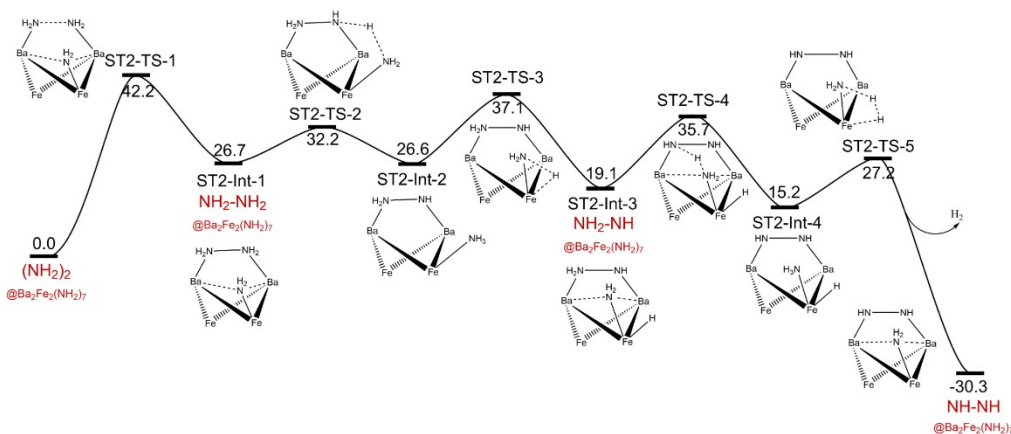


Figure S5. Structure of the Ba₂Fe₂(NH₂)₇ model (top view). Color scheme: Ba, green; N, blue; Fe, orange; H, white.

(a) Stage 1: $2 \times \text{NH}_3 \rightarrow 2 \times \text{NH}_2 + \text{H}_2$



(b) Stage 2: $2 \times \text{NH}_2 \rightarrow \text{NH}_2\text{-NH}_2 \rightarrow \text{NH-NH} + \text{H}_2$



(c) Stage 3: $\text{NH-NH} \rightarrow \text{N}_2 + \text{H}_2$

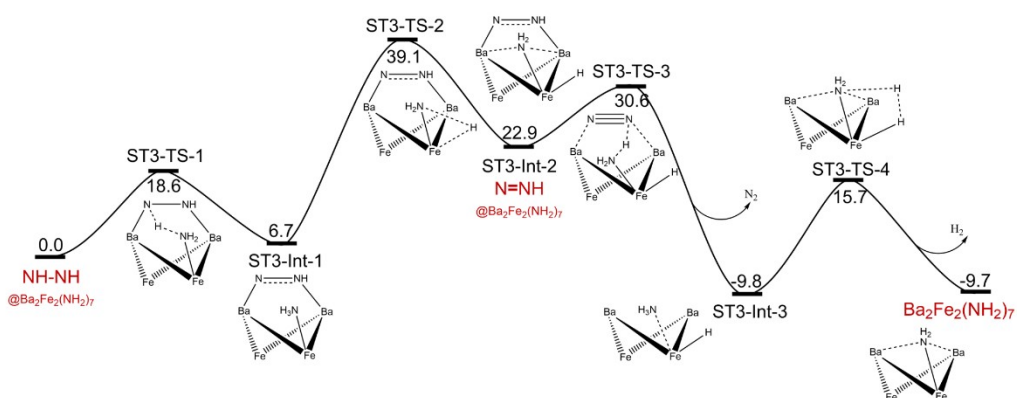


Figure S6. The structures of the intermediates and transition states in the reaction pathway shown in Figure 3. (a) Stage 1: from NH_3 to NH_2 ; (b) Stage 2: from NH_2 to NH-NH ; (c) Stage 3: from NH-NH to N_2 . Numbers in this profile indicate the free energy of each intermediate or transition state.

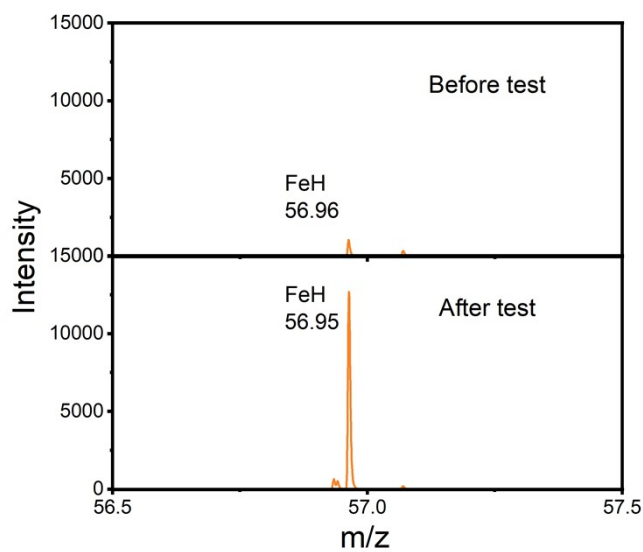


Figure S7. Partial negative ToF-SIMS spectra of the fresh and used Fe-Ba(NH₂)₂ catalyst (mass range m/z 56.5-57.5). It is seen that the intensity of FeH signal for the used sample is much higher than that of fresh sample.

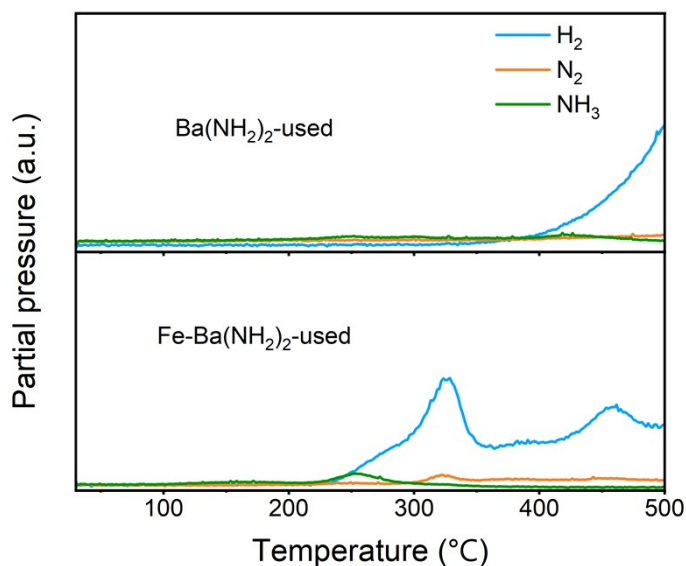


Figure S8. Temperature-programmed reaction of the 6wt%Fe-Ba(NH₂)₂ and Ba(NH₂)₂ samples after catalytic test under an argon flow. Ramping rate is 2 °C/min.

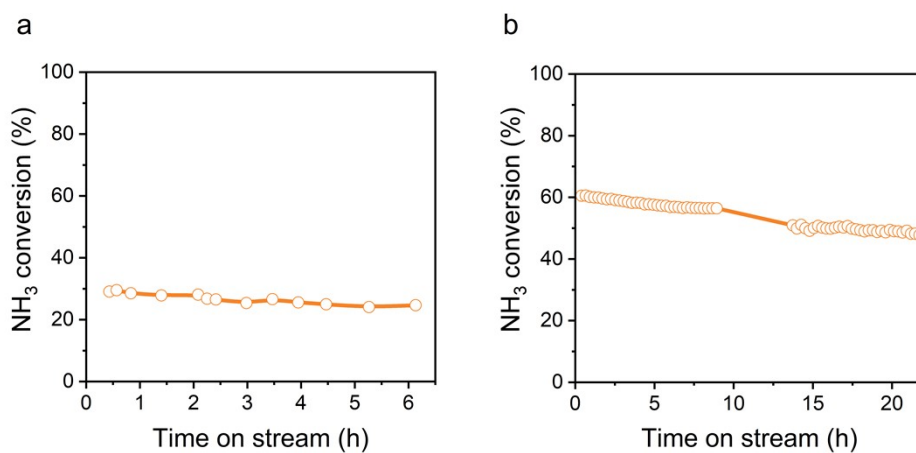


Figure S9. Ammonia conversion as a function of time on stream over 6wt%Fe-Ba(NH₂)₂.

a) Reaction conditions: 400 °C, pure NH₃, WHSV=6000 mL_{NH₃} g_{cat}⁻¹ h⁻¹. A slight decline in ammonia conversion can be observed over a period of 6 hours. b) Reaction conditions: 400 °C, 5% NH₃/Ar, WHSV=6000 mL g_{cat}⁻¹ h⁻¹.

Table S1. Selected reported non-noble metal-based catalysts for ammonia decomposition.

Catalyst	Metal content (wt%)	T (°C)	WHSV (mL $\text{g}_{\text{cat}}^{-1} \text{h}^{-1}$)	NH_3 conversion (%)	H_2 production rate ($\text{mmol g}_{\text{cat}}^{-1} \text{min}^{-1}$)	H_2 production rate ($\text{mmol g}_{\text{Fe}}^{-1} \text{min}^{-1}$)	TOF (s^{-1})
Fe-Ba(NH_2) ₂	6	400	6000	36	1.92	32	0.03
Fe-Ba(NH_2) ₂	1	400	6000	19.2	1.17	117	0.11
Fe-Ba(NH_2) ₂	1	400	30000	8.9	2.72	272	0.253
Fe-Ba(NH_2) ₂	1	400	60000	6.1	3.75	375	0.348
Fe-Ba(NH_2) ₂	1	400	120000	4.0	4.86	486	0.453
Ru/MgO ^[6]	3	400	36000	10	3.67	122.5	0.206
Fe-CNFs/mical ^[7]	3.5	450	6500	11	0.67	19.2	0.018
0.1Pt-10Fe/SiO ₂ ^[8]	10	500	12000	22	26.9	26.94	0.025
Fe/ZSM-5 ^[9]	5	450	30000	4	1.22	24.49	0.023
Fe ₂ N/CNTs ^[10]	15	400	6000	21	1.29	8.57	0.008
Fe ₂ O ₃ /CMK-5 ^[11]	5.2	450	7500	9	0.77	14.84	0.014
Fe ₃ O ₄ @CeO ₂ ^[12]	3.8	450	24000	19	4.65	122.4	0.11
Fe _{0.5} Cr _{0.5} ^[13]	52	400	22000	6	1.35	2.59	0.002
Fe ₂ O ₃ -50@pSiO ₂	42	400	15000	8	1.22	2.92	0.003
MgFeGaO ₄ ^[14]	28	400	120000(3%)	7	0.26	0.92	0.001
Fe ₂ O ₃ -SBA-15 ^[15]	31	550	15000	18	2.76	8.9	0.009
Fe/La-MgO ^[16]	20	500	22000	49	11	56	0.002

Fe@GC-3 ^[17]	9.56	450	6000	7	0.43	4.48	0.004
Ni-CaNH-HS ^[18]	10	400	15000	19	2.91	29.1	0.028
Ni-BaTiON ^[19]	5	400	15000	12.5	1.91	38.3	0.037
Ni-LaN ^[20]	5	400	15000	11	1.68	33.67	0.031
LaSrNiO ^[21]	26.8	400	30000	4	1.22	4.57	0.004
Co-CeO ₂ -3DOM ^[22]	4.8	400	6000	22	1.36	28.06	0.026
Co/CeO ₂ ^[22]	10	400	6000	16	0.98	9.8	0.009
Co/CYZ ^[23]	10	400	6000	18	1.1	11	0.011

Table S2. XPS atomic contents of Ba, Fe, N, C and O before and after Ar⁺ sputtering.

Etching depth	Ba (%)	Fe (%)	N (%)	C (%)	O (%)	Ba:Fe
0 nm	14.42	1.4	2.47	35.22	46.49	10.3:1
2 nm	24.73	3.07	4.17	15.14	52.89	8.1:1

Table S3. Calculated Gibbs free energy barrier heights of the two major steps in ammonia decomposition for some $Ba_xM_y(NH_2)_z$ species. Unit: kcal/mol.

Catalyst	First HAT Barrier Height (kcal/mol)	N-N Coupling Barrier Height (kcal/mol)
$Ba_2Fe_2(NH_2)_7$	17.4	42.2
$Ba_4(NH_2)_7$	43.3	35.2
$Ba_2Co_2(NH_2)_7$	34.6	43.2
$BaFe(NH_2)_7$	42.6	67.6

References

- [1] J. Hu, G. Wu, Y. Liu, Z. Xiong, P. Chen, K. Murata, K. Sakata, G. Wolf, *J. Phys. Chem. B* **2006**, *110*, 14688-14692.
- [2] P. Yu, H. Wu, J. Guo, P. Wang, F. Chang, W. Gao, W. Zhang, L. Liu, P. Chen, *J. Energy. Chem* **2020**, *46*, 16-21.
- [3] M. Nagib, H. Jacobs, H. Kistrup, *Kerntechnik* **1979**, *33*(1), 38-42.
- [4] J.-D. Chai, M. Head-Gordon, *Phys. Chem. Chem. Phys.* **2008**, *10*, 6615-6620.
- [5] M. Frisch, G. Trucks, H. Schlegel, G. Scuseria, M. Robb, J. Cheeseman, G. Scalmani, V. Barone, B. Mennucci, G. Petersson, in *Gaussian 09*, Gaussian Inc Wallingford, **2009**.
- [6] X. Ju, L. Liu, P. Yu, J. Guo, X. Zhang, T. He, G. Wu, P. Chen, *Appl. Catal. B Environ.* **2017**, *211*, 167-175.
- [7] X. Duan, G. Qian, X. Zhou, Z. Sui, D. Chen, W. Yuan, *Appl. Catal. B Environ.* **2011**, *101*, 189-196.
- [8] K. S. Indriadi, P. Han, S. Ding, B. Yao, S. Furukawa, Q. He, N. Yan, *Chinese. J. Catal.* **2023**, *50*, 297-305.
- [9] Z.-P. Hu, L. Chen, C. Chen, Z.-Y. Yuan, *Mol. Catal.* **2018**, *455*, 14-22.
- [10] H. Zhang, Q. Gong, S. Ren, M. A. Arshid, W. Chu, C. Chen, *Catal. Sci. Technol.* **2018**, *8*, 907-915.
- [11] A.-H. Lu, J.-J. Nitz, M. Comotti, C. Weidenthaler, K. Schlichte, C. W. Lehmann, O. Terasaki, F. Schüth, *J. Am. Chem. Soc.* **2010**, *132*, 14152-14162.
- [12] H.-Z. Cui, Y.-Q. Gu, X.-X. He, S. Wei, Z. Jin, C.-J. Jia, Q.-S. Song, *Sci. Bull.* **2016**, *61*, 220-226.
- [13] M. Du, L. Guo, H. Ren, X. Tao, Y. Li, B. Nan, R. Si, C. Chen, L. Li, *Nanomaterials* **2023**, *13*, 1280-1287.
- [14] K. F. Ortega, D. Rein, C. Lüttmann, J. Heese, F. Özcan, M. Heidelmann, J. Folke, K. Kähler, R. Schlögl, M. Behrens, *ChemCatChem* **2017**, *9*, 659-671.
- [15] J. C. Tseng, D. Gu, C. Pistidda, C. Horstmann, M. Dornheim, J. Ternieden, C. Weidenthaler, *ChemCatChem* **2018**, *10*, 4465-4472.
- [16] X.-C. Hu, W.-W. Wang, Z. Jin, X. Wang, R. Si, C.-J. Jia, *J. Energy. Chem* **2019**, *38*, 41-49.
- [17] L. Li, Q. Meng, W. Ji, J. Shao, Q. Xu, J. Yan, *Mol. Catal.* **2017**, *442*, 147-153.
- [18] K. Ogasawara, T. Nakao, K. Kishida, T.-N. Ye, Y. Lu, H. Abe, Y. Niwa, M. Sasase, M. Kitano, H. Hosono, *ACS Catal.* **2021**, *11*, 11005-11015.
- [19] K. Ogasawara, M. Miyazaki, K. Miyashita, H. Abe, Y. Niwa, M. Sasase, M. Kitano, H. Hosono, *Adv. Energy. Mater* **2023**, *13*, 2301286-2301299.
- [20] M. Miyazaki, K. Ogasawara, Y. Takekoshi, K. Miyashita, H. Abe, Y. Niwa, H. Hosono, M. Kitano, *Chem. Commun.* **2024**, *60*, 6447-6450.
- [21] X.-Y. Guo, J.-H. Wang, Q. Zhang, T.-Z. Li, H. Dong, C.-J. Jia, C. Li, Y.-W. Zhang, *Appl. Catal. B Environ.* **2024**, *348*, 123844.
- [22] C. Huang, Y. Yu, X. Tang, Z. Liu, J. Zhang, C. Ye, Y. Ye, R. Zhang, *Appl. Surf. Sci.* **2020**, *532*, 147335-147344.
- [23] C. Huang, H. Li, J. Yang, C. Wang, F. Hu, X. Wang, Z.-H. Lu, G. Feng, R. Zhang, *Appl. Surf. Sci.* **2019**, *478*, 708-716.